Frequenz, Vol. **65** (2011), pp. 261–265 DOI 10.1515/FREQ.2011.038

Imaging of Sources of Radiated Electromagnetic Interference

Johannes A. Russer[1,*] **and Peter Russer**[1]

[1] Institute for Nanoelectronics, Technische Universität München, Germany

Abstract. A method for imaging of the spatial distribution of sources of radiated electromagnetic interference is presented. By measurement the spatial correlations in the far-field of the radiated electromagnetic interference data are sampled that allow the reconstruction of the image of the radiation sources.

Keywords. Electromagnetics, electromagnetic compatibility, EMC, electromagnetic interference, EMI, noise.

PACS®(2010). 41.20.-q.

1 Introduction

Stochastic electromagnetic fields play an important role in wireless communications, in sensorics and in electromagnetic interference (EMI) [10]. Their random fluctuations may either originate from thermal noise or from electromagnetic interference originating from specific transmitters. In communications and in most sensorics applications, stochastic electromagnetic signals are interfering signals, degrading the signal to noise plus interference ratio of systems. In some cases, as for example in radiometry, stochastic signals may contain the desired information.

Due to the high bandwidth and their low power levels, modern electronic systems are highly sensitive to electronic disturbances. The design of electronic systems requires the consideration of active and passive electromagnetic compatibility (EMC), i.e. the emission of equipment should not disturb other equipment, and that equipment should not be disturbed by other equipment.

Broad-band measurement systems for the measurement of electromagnetic interference are important tools required in the development of electric and electronic products and for the test of their electromagnetic compliance [11]. Today, time domain electromagnetic interference measurement systems that use ultra high-speed analog-to-digital converters and real-time digital signal processing systems enable ultra fast tests and measurements for electromagnetic compliance for frequencies up to 26 GHz [2, 8].

EMI/EMC modeling of packaged electronics requires space resolution of the emitted electromagnetic interference in order to facilitate an accurate modeling of the EMI emitted into the environment [4, 10]. In [10], we have shown that the correlation of the noise and/or interference sources has a strong influence on the spatial distribution on the radiated electromagnetic interference. A radiating device with several internal noise sources of arbitrary mutual correlation can be fully characterized by two–point scanning of the tangential electric or magnetic field in a Huygens surface enclosing the device. Two-point scanning means that the field amplitudes are measured in every pair of field sampling points and the correlation spectra are determined for each pair of sampling points.

The correlation of radiated electromagnetic interference, measured simultaneously in two different points is already done in the context of ambient cancellation techniques in time-domain EMI measurements [5,6]. In the ambient noise canceling time-domain EMI measurement system, two interference signals are received by two broad-band antennas, where the first antenna is receiving predominantly the EMI radiated from the device under test and a second antenna receives predominantly the ambient noise. This technique allows fast measurements of EMI in the time-domain at open area test sites and can also be applied for the measurement of the mutual field correlation in a large set of pairs of sampling points. Since modern time-domain EMI measurement systems, compared with traditional EMI measurement systems, yield reduction of the measurement time by a factor of up to 8000 [1], two-point scanning of a large number of sampling point pairs is feasible.

In this work we discuss the possibility of the imaging of noise and EMI scenarios by two-point sampling. Sampling of the two-point correlations in a *Fourier plane*, distant from the object plane yields the information required for the digital reconstruction of the image of the sources [7]. In Section 2, we discuss the imaging by a lens. Based on these considerations we develop a method for computational image reconstruction in Section 3. Coherent electromagnetic waves are propagating from the object plane to the Fourier plane where the waves are sampled and digitally processed. In Section 4, the free space propagation of incoherent waves from the object plane to the Fourier plane is discussed. The discrete Fourier transform (DFT) is applied to the processing of sampled fields in Section 5. A numerical example for the image reconstruction of an incoherent source distribution in the object plane is discussed in Section 6.

Corresponding author: Johannes A. Russer, Institute for Nanoelectronics, Technische Universität München, Arcisstr. 21, 80333 Munich, Germany; E-mail: jrusser@tum.de.

Received: July 21, 2011.

2 Fourier Optics

In this section we discuss the image reconstruction by sensing the far-field emitted from a coherently illuminated object plane.

Let us first consider the conventional imaging system with a lens shown in Figure 1. Within the Fresnel approximation the free-space propagation of the wave from the object plane to the lens plane is described by [7, p. 60]

$$\Psi_{\mathrm{L1}}(x,y) = \frac{\mathrm{e}^{jkd}}{j\lambda d}\mathrm{e}^{j\frac{k}{2d}(x^2+y^2)} \times \iint_{-\infty}^{\infty} \mathrm{e}^{j\frac{k}{2d}(x'^2+y'^2)}\Psi_{\mathrm{O}}(x',y')\mathrm{e}^{-\frac{2\pi j}{\lambda d}(xx'+yy')}dx'dy'. \tag{1}$$

Apart from multiplicative amplitude and phase factors that are independent from x' and y' the field distribution in front of the lens plane, $\Psi_{\mathrm{L1}}(x,y)$, is the two-dimensional Fourier transform of $\exp[j(k/2d)(x'^2+y'^2)]\Psi_{\mathrm{O}}(x',y')$. The Fourier transform is performed at the space frequencies $x'/\lambda d$ and $y'/\lambda d$.

In the paraxial approximation, a thin lens with focal length f, thickness w, and refractive index n, transforms the field in front of the lens, $\Psi_{\mathrm{L1}}(x,y)$, into the field behind the lens, $\Psi_{\mathrm{L2}}(x,y)$ [7, p. 80],

$$\Psi_{\mathrm{L2}}(x,y) = \mathrm{e}^{jknw}\mathrm{e}^{-j\frac{k}{2f}(x^2+y^2)}\Psi_{\mathrm{L1}}(x,y)\,. \tag{2}$$

The lens performs a phase delay of the incident wave, depending on the radius $r = \sqrt{x^2+y^2}$. The phase delay is maximum for $r = 0$ and decreases, proportionally to r^2. If the object plane is in the focal plane of the lens, i.e. $d = f$, a spherical wave originating from a point in the object plane will be transformed into a plane wave. For $1/d + 1/b = 1/f$, the lens will change and reverse the curvature of the spherical wave such that it converges into a point in the image plane.

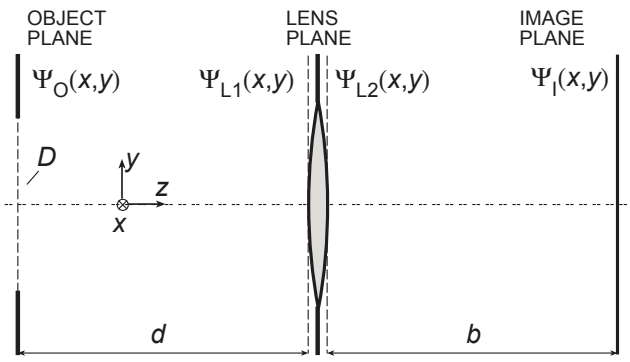

Figure 1. Imaging system.

For the case $d = f$, where the object plane is the focal plane of the lens, we obtain from (1) and (2)

$$\Psi_{\mathrm{L2}}(x,y) = \frac{\mathrm{e}^{jk(d+nw)}}{j\lambda d} \times \iint_{-\infty}^{\infty} \mathrm{e}^{j\frac{k}{2d}(x'^2+y'^2)}\Psi_{\mathrm{O}}(x',y')\mathrm{e}^{-\frac{2\pi j}{\lambda d}(xx'+yy')}dx'dy'. \tag{3}$$

The term $\exp[jk(d+nw)]$ represents the constant phase delay due to the wave propagation along the distance $d+nw$ and can be dropped. The factor $\exp[j(k/2d)(x'^2+y'^2)]$ can be eliminated by replacing the object plane by a spherical surface with a curvature radius f. We also omit the scale factor $1/j\lambda d$. In this case the optical system consisting of the free wave propagation space between object plane and the thin lens, can be described by the approximation:

$$\Psi_{\mathrm{L2}}(x,y) \approx \iint_{-\infty}^{\infty} \Psi_{\mathrm{O}}(x',y')\mathrm{e}^{-\frac{2\pi j}{\lambda d}(xx'+yy')}dx'dy'. \tag{4}$$

In this approximation, the field $\Psi_{\mathrm{L2}}(x,y)$ behind the lens is the Fourier transform of the object plane field $\Psi_{\mathrm{O}}(x',y')$.

3 Computational Image Reconstruction

In the following we describe a method for the computational construction of the image of radiating sources arranged in a plane by scanning the far-field emitted from the sources. Figure 2 shows the considered geometry. In the object plane (OP), positioned in the xy-plane at $z = 0$, radiating sources are positioned. The distribution of the radiating sources is described by the scalar field $\Psi_{\mathrm{O}}(x',y')$, which is proportional to the impressed electric polarization in z-direction. The coordinates in the object plane are x' and y'. In a parallel plane at $z = d$, called Fourier plane, the field is scanned. We consider Hertzian dipole sources in the object plane oscillating in y-direction only. Furthermore, we assume the distance d to be large compared with the transverse extensions of object plane and the Fourier plane, and the dimensions of these planes large compared with the wavelength λ. Under these assumptions the electric field in the Fourier plane exhibits only a y-component and can be described by a scalar field $\Psi_{\mathrm{F}}(x,y)$.

The field, scanned in the Fourier plane corresponds to the field $\Psi_{\mathrm{L1}}(x,y)$ according to (1). We can easily obtain the field $\Psi_{\mathrm{L2}}(x,y)$ by applying to the field amplitude sampled in the point (x,y) a phase delay depending on the sampling point coordinates according to (2). This correction depends on the focal distance f. Applying this correction focuses the *virtual lens* on an object plane in distance $d = f$. Objects in a focal plane with distance $d = f$ can be imaged with maximal resolution. Different from the case of a real

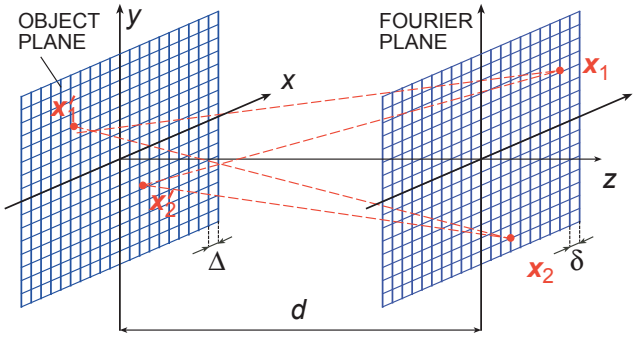

Figure 2. Object plane and Fourier plane.

lens, data processing can be performed for the virtual lens with the same set of sampled data for different focal lengths.

With the lens correction and under the assumptions discussed at the end of Section 2, the field distribution behind the virtual lens, $\Psi_F(x, y)$, is represented by the Fourier integral

$$\Psi_F(x, y) = \iint_{-\infty}^{\infty} e^{-\frac{2\pi j}{\lambda d}(xx'+yy')} \Psi_O(x', y')dx'dy'. \quad (5)$$

Sensing amplitude and phase of the wave in the Fourier plane allows for the reconstruction of the original picture in the object plane by applying the inverse Fourier transform

$$\Psi_O(x', y') = \iint_{-\infty}^{\infty} e^{\frac{2\pi j}{\lambda d}(xx+yy')} \Psi_F(x, y)dxdy. \quad (6)$$

4 Stochastic Sources

If the sources in the object plane are stochastic, as for example thermal noise sources or EMI sources, numerical computations cannot be done on the basis of amplitude spectra. In case of a stochastic field the spectral energy densities and the field correlation in the object plane and the Fourier plane can be described by the correlation spectra [10]. We introduce the *correlation spectrum* of the field amplitudes at the points (x_1, y_1) and (x_2, y_2) by

$$\Gamma_i(x_1, y_1; x_2, y_2) = \lim_{T\to\infty} \frac{1}{2T} \langle \Psi_{iT}(x_1, y_1)\Psi^*_{iT}(x_2, y_2)\rangle, \quad (7)$$

where $i = O, F$, the brackets $\langle\cdot\rangle$ denote the ensemble average and the subscript T denotes that the spectrum is taken from a signal, which is time-windowed in the interval $[-T, T]$. For $(x_1, y_1) = (x_2, y_2)$, the spectrum $\Gamma_i(x_1, y_1; x_1, y_1)$ is called the *autocorrelation spectrum*, otherwise $\Gamma_i(x_1, y_1; x_2, y_2)$ is called the *cross correlation spectrum*. The autocorrelation spectrum expresses the spectral energy density of the field in a certain point. The evaluation of the superposition of stochastic fields requires also the knowledge of the cross correlation spectra. Inserting (5) into (7) yields the transformation formula for the correlation spectra from the object plane into the Fourier plane,

$$\Gamma_F(x_1, y_1; x_2, y_2) = \iiiint_{-\infty}^{\infty} e^{-\frac{2\pi j}{\lambda d}(x_1x'_1-x_2x'_2+y_1y'_2-y_1y'_2)} \times \Gamma_O(x'_1, y'_1; x'_2, y'_2)dx'_1dy'_1dx'_2dy'_2. \quad (8)$$

This transformation is described by a four-dimensional Fourier integral, since all point-to-point correlations have to be considered in the object plane as well as in the Fourier plane. The inverse transformation is given by

$$\Gamma_O(x'_1, y'_1; x'_2, y'_2) = \iiiint_{-\infty}^{\infty} e^{\frac{2\pi j}{\lambda d}(x_1x'_1-x_2x'_2+y_1y'_2-y_1y'_2)} \times \Gamma_F(x_1, y_1; x_2, y_2)dx_1dy_1dx_2dy_2. \quad (9)$$

If the sources in the object plane exhibit a fine-grained statistical independence in that way that the field amplitudes at different points in the object plane are completely uncorrelated, the correlation spectrum of the field in the object plane is given by

$$\Gamma_O(x_1, y_1; x_2, y_2) = F_O(x_1, y_1)\delta(x_1 - x_2)\delta(y_1 - y_2), \quad (10)$$

where F_O is a spectral density function. In this case the correlation spectrum in the Fourier plane is represented by

$$\Gamma_F(x_1, y_1; x_2, y_2) \equiv \Gamma_F(x_1 - x_2, y_1 - y_2) = \iint_{-\infty}^{\infty} e^{-\frac{2\pi j}{\lambda d}((x_1-x_2)x'_2+(y_1-y_2)y'_2)} F_O(x'_1, y'_1, \omega)dx'_1dy'_1. \quad (11)$$

In this special case, for the reconstruction of the original image, we don't need to scan the correlation of all pairs of points in the Fourier plane. It will be sufficient to measure the correlations between all sampling points and a single reference point. In the case of a number of s sampling points, we only have to make s measurements instead of $s(s-1)/2$ measurements.

5 Discrete Fourier Transform

To measure the field distribution in the Fourier plane we introduce a grid and measure the two-point correlations in pairs of grid points. The measurements can be performed using a two-channel time-domain EMI measurement system as described in [5]. For image reconstruction, we introduce a grid in the object plane. The field samples in the object plane and in the Fourier plane are related by two-dimensional discrete Fourier transforms (DFTs). Very efficient DFT algorithms are available for the case $N = 2^l$ with integer l [3, 9].

Let us introduce in the object plane as well as in the Fourier plane grids with dimensions $N \times N$. Let both grids be quadratic with side lengths w_O in the object plane, and w_F in the Fourier plane. The discretization intervals in the object and Fourier planes, Δ and δ, respectively are given by $w_\mathrm{O} = N\Delta$ and $w_\mathrm{F} = N\delta$. The discretization interval of the grid in the Fourier plane is related to the width w_O of the grid in the object plane by $\delta = \lambda d / w_\mathrm{O}$.

We note that for a given width w_O of the grid in the object plane the length of the discretization interval is proportional to the wavelength λ. This has to be considered when measurements are made for a broad frequency band. If today's most efficient time-domain EMI measurement systems are used for the measurement of the correlation spectra, in a single two-point measurement, the autocorrelation spectrum is obtained for a broad frequency band. From the grid used for the measurement, by interpolation, a virtual grid has to be established fulfilling $\delta = \lambda d / w_\mathrm{O}$ for every frequency.

We introduce space-discrete field sample values $\tilde{\Psi}_\mathrm{O}[m,n] = \Psi_\mathrm{O}(m\Delta, n\Delta)$, $\tilde{\Psi}_\mathrm{F}[m',n'] = \Psi_\mathrm{F}(m'\delta, n'\delta)$, which are related to each other by the discrete Fourier transforms

$$\tilde{\Psi}_\mathrm{F}[m,n] = \sum_{m,n=0}^{N-1} \tilde{\Psi}_\mathrm{O}[m',n'] \mathrm{e}^{-\frac{2\pi j}{N}(mm'+nn')}, \tag{12a}$$

$$\tilde{\Psi}_\mathrm{O}[m,n] = \frac{1}{N^2} \sum_{m',n'=0}^{N-1} \tilde{\Psi}_\mathrm{F}[m',n'] \mathrm{e}^{\frac{2\pi j}{N}(mm'+nn')}. \tag{12b}$$

The discrete Fourier transform of the correlation spectrum is given by

$$\tilde{\Gamma}_\mathrm{F}[m_1,n_1;m_2,n_2] = \sum_{\substack{m_1',n_1',\\ m_2',n_2'=0}}^{N-1} \tilde{\Gamma}_\mathrm{O}[m_1',n_1';m_2',n_2'] \times \mathrm{e}^{-\frac{2\pi j}{N}(m_1m_1'-m_2m_2'+n_1n_1'-n_2n_2')}, \tag{13}$$

and the inverse transformation is

$$\tilde{\Gamma}_\mathrm{O}[m_1',n_1';m_2',n_2'] = \frac{1}{N^4} \sum_{\substack{m_1,n_1,\\ m_2,n_2=0}}^{N-1} \tilde{\Gamma}_\mathrm{F}[m_1,n_1;m_2,n_2] \times \mathrm{e}^{\frac{2\pi j}{N}(m_1m_1'-m_2m_2'+n_1n_1'-n_2n_2')}. \tag{14}$$

6 Examples

Let us first consider the two uncorrelated radiation sources at the elementary example of two incoherent radiation sources, both with intensity I_0, and located at the points $(-x_0, 0)$ and $(x_0, 0)$. In that case the autocorrelation spectrum in the object plane is given by

$$\Gamma_\mathrm{O}(x_1,y_1;x_2,y_2) = I_0\delta(x_1-x_0)\delta(x_2-x_0)\delta(y_1)\delta(y_2) + A_0\delta(x_1+x_0)\delta(x_2+x_0)\delta(y_1)\delta(y_2). \tag{15}$$

Inserting this into (8) yields the correlation spectrum of the field in the Fourier plane

$$\Gamma_\mathrm{F}(x_1,y_1;x_2,y_2) = 2I_0 \cos\left[\frac{2\pi}{\lambda d}(x_1-x_2)x_0\right]. \tag{16}$$

We note that the intensity distribution in the Fourier plane, given by $\Gamma_\mathrm{F}(x,y;x,y) = 2I_0$, is a constant, and an amplitude function is not available. However, applying the two-point correlation spectrum in the Fourier plane, given in (16), allows to reconstruct the image of the source distribution in the object plane.

Now, let us consider five uncorrelated point-like sources at positions in the object plane and with intensities $\tilde{I}[m,n] = \tilde{\Gamma}_\mathrm{O}[m,n;m,n]$ listed in Table 1. Due to the lack of correlation, the correlation spectrum exhibits only elements with $m_2 = m_1$ and $n_2 = n_1$. The discretization in the object plane is performed with a grid of size 100×100.

Figure 3 shows the intensity distribution of the incoherent and uncorrelated sources in the object plane. We have to sample the two-point correlations in the Fourier plane for the construction of the image of the source distribution. Due to the incoherence of the sources, the intensity distribution in the Fourier plane is constant and we have only to sample

$\tilde{\Gamma}_\mathrm{O}[15,60;15,60] = 0.8I_0$
$\tilde{\Gamma}_\mathrm{O}[20,45;20,45] = 0.7I_0$
$\tilde{\Gamma}_\mathrm{O}[50,80;50,80] = 1.0I_0$
$\tilde{\Gamma}_\mathrm{O}[65,10;65,10] = 0.5I_0$
$\tilde{\Gamma}_\mathrm{O}[75,75;75,75] = 1.0I_0$

Table 1. Incoherent sources.

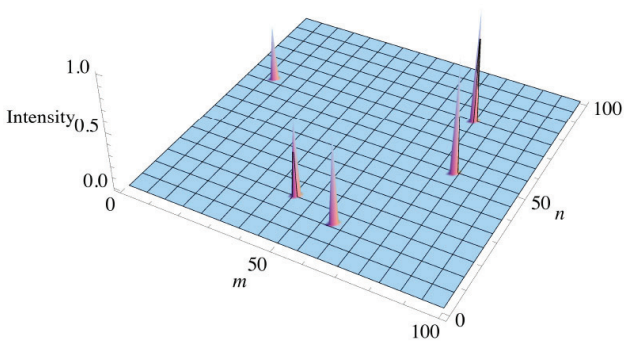

Figure 3. Intensity distribution in the object plane.

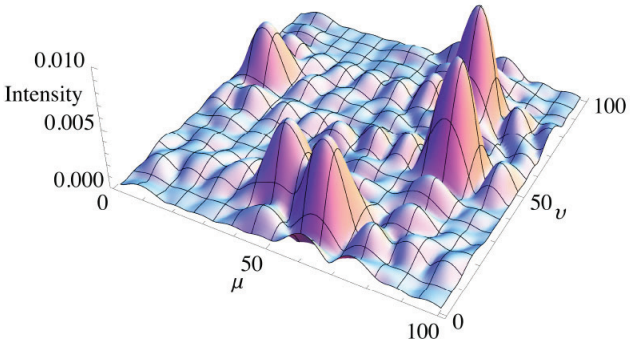

Figure 4. Reconstruction of the intensity distribution in the object plane.

the field correlations between the chosen set of sampling points and one selected point of reference. Choosing a set of 10×10 sampling points we perform a two-dimensional rectangular windowing in the Fourier plane. Figure 4 shows the reconstructed image of the source distribution. The restriction to 10×10 sampling points yields a broadening of the width of the sources. However, it still allows us to localize and separate the source points.

7 Conclusion

In this work we have presented a method of image reconstruction of the spatial distribution of stochastic electromagnetic radiation sources from a two-point scanning in the far-field. The measurement effort is feasible if modern time-domain EMI measurement systems are applied. The image reconstruction allows to construct an image of the source distribution. Since the focal plane can be chosen during the processing of the data, a three-dimensional imaging of the source distribution will be possible to some extent. For a sufficiently large measurement basis in the Fourier plane, also stereoscopic methods can be applied to achieve the goal of three-dimensional source modeling.

In the given examples we have restricted our considerations to incoherent sources. However the method is applicable also to correlated and partially correlated sources. In this case the field distribution in the Fourier plane will be non-uniform and we have to take two-point samples of the correlation spectrum in all $n(n-1)/2$ pairs of n sampling points. Also this will be feasible with time-domain EMI measurement systems, if the field probes are either switched and arranged in a matrix or are positioned sufficiently fast.

The described method allows to measure the spatial distribution of noise sources in objects. The intensity and mutual correlation of noise sources can be analyzed. The Frequency dependence of these parameters can be displayed, and ambient noise and interference can easily be separated from the noise and interference radiated by the object under test.

Acknowledgments

This work has been supported by the Deutsche Forschungsgemeinschaft.

References

[1] Stephan Braun, Arnd Frech and Peter Russer, A low-noise realtime time-domain EMI measurement system, in: *Electromagnetic Compatibility, 2007. EMC Zurich 2007. 18th International Zurich Symposium on*, pp. 381–384, 2007.

[2] Stephan Braun and Peter Russer, A low-noise multiresolution high-dynamic ultra-broad-band time-domain EMI measurement system, *Microwave Theory and Techniques, IEEE Transactions on* **53** (2005), 3354–3363.

[3] E. Oran Brigham, *The Fast Fourier Transform*, Prentice-Hall, 1974.

[4] Andreas C. Cangellaris and Johannes A. Russer, EMI/EMC modeling of packaged electronics: challenges and opportunities, *Proceedings of the 30th URSI General Assembly 2011, Istanbul, Turkey, 13–20 August 2011* (2011).

[5] Arnd Frech, Stephan Braun and Peter Russer, Time-domain EMI measurements in the presence of ambient noise, in: *Proceedings of the 2008 IEEE International Symposium on Electromagnetic Compatibility*, pp. 139–142, 2009.

[6] Arnd Frech, A. Zakaria, Stephan Braun and Peter Russer, Ambient noise cancelation with a time-domain EMI measurement system using adaptive filtering, in: *Electromagnetic Compatibility and 19th International Zurich Symposium on Electromagnetic Compatibility, 2008. APEMC 2008. Asia-Pacific Symposium on*, pp. 534–537, 2008.

[7] Joseph W. Goodman, *Introduction to Fourier Optics*, McGraw-Hill, New York, 1968.

[8] Christian Hoffmann, Alexander Boege and Peter Russer, A low-noise time-domain EMI measurement system for measurements up to 26 GHz, *Proceedings of the 30th URSI General Assembly 2011, Istanbul, Turkey, 13–20 August 2011* (2011).

[9] Alan V. Oppenheim and Ronald W. Schafer, *Discrete-Time Signal Processing*, 2 ed, Signal Processing Series, (Prentice-Hall, 1989.

[10] Johannes A. Russer and Peter Russer, An Efficient Method for Computer Aided Analysis of Noisy Electromagnetic Fields, in: *2011 IEEE MTT-S International Microwave Symposium Digest, June 5th–10th, Baltimore, MD, USA*, 2011.

[11] Peter Russer, EMC measurements in the time-domain, *Proceedings of the 30th URSI General Assembly 2011, Istanbul, Turkey, 13–20 August 2011* (2011).